Materials Today Communications 38 (2024) 107881

Contents lists available at ScienceDirect

Materials Today Communications

journal homepage: www.elsevier.com/locate/mtcomm

Comprehensive study of microstructure, phase transformations, and mechanical properties of nitinol alloys made of shape memory and superelastic wires and a novel approach to manufacture Belleville spring using wire arc additive manufacturing

Ajit Kumar [a,*], Iyamperumal Anand Palani [a], Muralidhar Yadav [b]

[a] Department of Mechanical Engineering, Indian Institute of Technology Indore, Indore 453552, India
[b] Department of Materials Engineering, Indian Institute of Science Bangalore, Bengaluru 560012, India

ARTICLE INFO

Keywords:
Wire arc additive manufacturing
Nitinol
Superelasticity
Shape memory effect
Mechanical properties

ABSTRACT

In the present work, using wire arc additive manufacturing (WAAM), a novel approach is implemented to manufacture the Belleville spring/washer made from superelastic (SE) and shape memory (SM) Nitinol (NiTi) wires. A detailed correlation between the chemical composition, microstructure, and martensite transformation of deposited layers and their mechanical properties has been established. The energy dispersive spectroscopy (EDS) results revealed that the first track deposited using both SE and SM effect wire consisted of significant Fe constituents, which was further reduced while increasing the number of tracks. Moreover, as compared to the sample manufactured with SE effect NiTi wire (S1), the X-ray diffraction (XRD) of the sample manufactured with SM effect NiTi wire (S2) showed a secondary phase like $NiTi_2$ along with the major NiTi ($B19'$ martensitic). It has been found that the presence of Ni_4Ti_3 precipitate in the microstructure of SE causes an enhanced superelasticity desired for the Belleville spring applications. Furthermore, the mechanical properties, microstructure, and phase transformation temperature of both S1 and S2 were investigated and compared. It was found that S2 has a finer microstructure than S1. Also, the compressive strength and hardness of S2 were higher than that of S1. In contrast, the tensile strength of the S2 was found to be lower than the S1. Regarding manufacturing the Belleville spring using WAAM, S1 showed promising mechanical and martensitic transformation results.

1. Introduction

Nitinol (NiTi) exhibits a unique functional property due to its superelastic (SE) and shape memory (SM) effect. NiTi alloys can deform strongly and return to their original form when mechanically relieved (SE) or heated to a standard temperature (SM) [1]. With continuous improvements in product quality and reduced production costs, these alloys have become desirable alternatives to conventional metallic alloys in a wide range of fields, including biomedical, mechanical, and civil engineering [2–4]. Recent studies have investigated NiTi alloys for innovative springs due to their unique properties, such as tuneable behavior, temperature-dependent properties, high recovery, and high damping abilities [5,6]. Nevertheless, due to their hardening and elasticity, nitinol components with complex geometries are difficult to machine and fabricate using conventional methods [7,8]. With the advent of additive manufacturing, it is now possible to produce complex items. Many processing routes have been explored to process NiTi alloys, and most of these routes have revolved around lasers [9–11], electrical resistance [12], Tungsten Inert Gas (TIG) [13], or ultrasound [14,15] for treating relatively simple geometries.

In recent times, mostly, laser [16,17] or electron beam [18–20] systems are being utilised to produce additively manufactured shape memory alloys (SMAs) by generating abundant heat in the powder bed. However, slow production rates with high equipment and powder feedstock costs are some of the shortcomings of laser and electron beam powder-based additive manufacturing (PBAM) processes to produce NiTi components, as reported by Elahinia et al. [7,21]. As powder-bed systems are more likely to show flaws, such as porosity or lack of fusion [22], PBAM also fails to evaluate the properties of NiTi components under tensile conditions. Eventually, Wire and arc additive

* Corresponding author.
E-mail address: ajitk.iitdelhi@gmail.com (A. Kumar).

https://doi.org/10.1016/j.mtcomm.2023.107881
Received 25 September 2023; Accepted 14 December 2023
Available online 18 December 2023

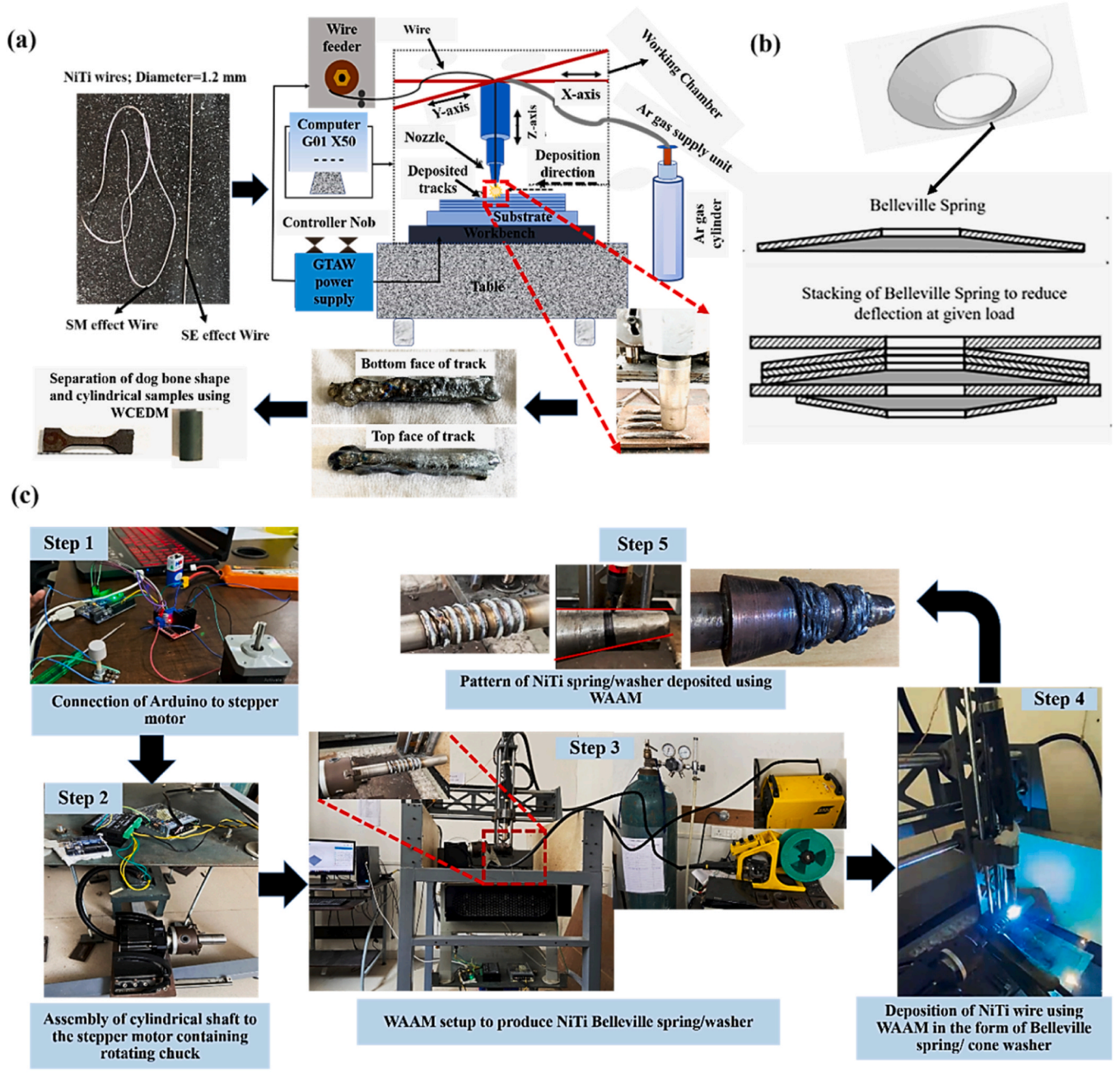

Fig. 1. (a) Schematic diagram of NiTi track deposited using WAAM, (b) a pictorial view of the Belleville spring with its stacking arrangement, and (c) step-by-step presentation to manufacture a prototype of a Belleville spring using WAAM.

manufacturing (WAAM) showed a promising additive manufacturing technique to produce NiTi components with minimal defect at the optimized process parameters, cheap and higher deposition rate, higher sample production, and more affordable equipment cost compared to powder-based methods [23,24]. WAAM can, therefore, be used for additively manufactured nitinol parts in both compression [25] and tension [26–28] evaluations, making it ideal for high-performance applications, especially in the automotive and aerospace industries.

Compositions and structures of the final components are susceptible to minute changes since their properties largely depend on their original chemical compositions and processing histories. Increasing the Ni content in NiTi alloys by as little as one atomic % can result in a temperature change of more than 100 °C during the onset of martensite transformation [29]. Properties can also be altered by minor impurities or oxygen. Commercially available nitinol wires are preferred as feedstock materials for determining the exact composition of the components. In a recent study, a dual wire feeder was used to print the Nitinol on the titanium substrate by Wang et al. [28]. The GTAW process was used in the work to melt pure Ti and Ni wires to deposit NiTi alloy with 53.5 at% Ni on the Ti substrate. The sample structure was heterogeneous and contained the NiTi matrix, with Ni-rich precipitates such as Ni_4Ti_3 and Ni_3Ti. The study on the martensitic transformations in different parts of the Ni-rich NiTi sample by differential scanning calorimetry has shown the presence of very weak peaks of heat release and heat absorption. This indicated that the martensitic transformations were partially suppressed; hence, the alloy with such a structure would not be able to demonstrate good functional behavior. One of the possible reasons for the heterogeneous system of the WAAM sample produced in this study might be the use of elemental Ti and Ni wires instead of NiTi alloy wire. Furthermore, anisotropic microstructures and precipitation of different

phases reduce ductility and increase hardness and tensile strength. To address the shortcomings in the above study, 5-layered NiTi alloy was fabricated on the Ti substrate using the $Ni_{50.9}Ti_{49.1}$ wire as the feedstock via the GMAW process for the first time and given the layer-by-layer study on the microstructural evolution, grain size variation, composition variation of Ni across the different layers and its role on the interpretation of the transformation temperature were also studied by Resnina et al. [30]. Based on the results, the Ti-rich NiTi alloys dominated the 2nd layer, whereas Ni-rich NiTi alloys dominated the 3rd and 4th layers. As a result of the Ti-rich NiTi layer, the shape memory effect was two times greater than with a Ni-rich NiTi layer alone. Because the layer was Ti-rich, the stress-induced martensite persisted even after removing the load, suppressing superelasticity. In another study, Ponikarova et al. [31], examined the effects of arc voltage and substrate type on the functional properties and structure of parts made with $Ni_{50.9}Ti_{49.1}$ wire using the WAAM was examined. A Ni-rich NiTi wire deposited on a Ti substrate exhibits shape memory characteristics at high temperatures, resulting in a martensitic NiTi wall. It was reported that increasing the arc voltage did not affect shape memory behavior but significantly decreased the strain up to failure. A solid solution of NiTiFe and precipitates of Ti-C, Ni_4Ti_3, and Ni_3Ti_2 formed on the steel substrate as the first layer formed. The Fe concentration in the solid solution of NiTiFe increased as the arc voltage increased. The iron concentration in the NiTi sample decreased during subsequent layer deposition but remained above 1.5 at%, suppressing martensitic transform and shape memory effects. When Singh et al. [32] varied the number of laser passes during laser marking, they found a corresponding increase in channel depth and a decrease in track width. Furthermore, NiTi layers deposited with WAAM over laser-marked areas have increased strength due to finer grains, reduced porosity, and Ni-rich phases. In their study, Zeng et al. [22] reported that the microstructure of NiTi parts deposited using Ni-rich wire with WAAM turned into equiaxed from columnar as it reached the top layer due to the different thermal cycle conditions. Reports indicate that NiTi parts fabricated with WAAM exhibit promising superelastic behavior, demonstrating the potential of this technique for fabricating complex NiTi components.

The above literature shows that extensive research has been performed for the NiTi SMA fabricated using WAAM. Yet, no reports have evaluated the simultaneous findings of the microstructure, phase transformations, and mechanical properties (compression, tension, and hardness) of NiTi alloys fabricated with WAAM using both SE and SM effect wires. Concerning the fabrication of a Belleville spring from NiTi alloys with the desired properties, the work aims to perform a comparative study between the microstructure, phase transformations, and mechanical properties of NiTi alloys fabricated using WAAM with the wires possessing SE and SM characteristics. The novelty of the current work includes (1) a successful attempt in making Belleville spring using NiTi via wire arc additive manufacturing processing route for the very first time, (2) superelastic and shape memory nitinol printing, their process parameter optimization, and their property evaluation for the first time (3) a thorough processing-structure-property correlation and comparison for the wire arc additively manufactured superelastic and shape memory nitinol. The current study is expected to provide valuable information to the researchers and industries for successfully printing Belleville spring using wire arc additive manufacturing method compared to the conventionally existing methods. Furthermore, using WAAM for making such springs will be beneficial in cost saving for the industries, and using nitinol for applications whose superelastic properties will add more value to the printed spring.

2. Experimental procedure

2.1. Materials and methods

Nitinol wires (Ø1.2 mm) made of the SE ($Ni_{53}Ti_{47}$ wt%) and SM effect ($Ti_{51.2}Ni_{48.8}$ wt%) were taken as feedstock materials in this study (Supplementary files of SE wire (Video F1) and SM (Video F2). The elemental composition of the chosen wires was obtained using energy dispersive spectroscopy (EDS) analysis. A wire feeder coupled to the X-Y table feeds the feedstock wire to the welding flame. The X-Y table has an electrode that allows movement in a different direction. G and M codes are used to program the X-Y control, supported by the Repitier host software. A WAAM technique based on Gas Metal Arc Welding (GMAW) was used to deposit these wires on the substrate (Video F3). A schematic flow diagram of the NiTi specimens fabricated using WAAM is shown in Fig. 1. Although the first deposited track had significant cracks on the surface, the third layer was considered for the study. To deposit uniform layers of the NiTi alloys using SE and SM effects wire, tracks were deposited with different process parameters. This section discussed the process parameters and their responses (uniform deposition) based on preliminary experiments. The present work started with pilot experiments considering the main process parameters such as arc voltage, wire feed speed, nozzle speed, and gas flow rate. Since NiTi is an expensive and scarce material, several process parameters were optimized to obtain defect-free parts. Table 1 shows the optimal process parameters for WAAM to get a smooth and uniform layer of NiTi alloys with SE and SM effect wires. The process parameters used to deposit uniform tracks using SM effect NiTi wire were not as suitable as the deposition of tracks using SE effect NiTi wire because the wire was crumpled at the entrance of the wire inline in the case of tracks deposition using SM effect NiTi wire. A uniform track of SM effect NiTi wire was achieved with the values given in Table 1 by choosing different settings.

Table 1
Optimal process parameters of WAAM to deposit SE and SM effect NiTi wires.

Deposition of NiTi tracks using	Process parameters			
	Arc voltage (V)	Wire feed rate (m/min)	Torch speed (mm/min)	Gas flow rate (Lit/min)
SE effect wire	17	5	300	20
SM effect wire	18.5	5.8	300	20

After conducting the comparative study between the microstructural, mechanical, and phase transformation properties, a novel approach shown in Fig. 1c was attempted to fabricate the prototype of Belleville spring (see Fig. 1b) with NiTi wire using WAAM. The fabrication of Belleville spring with conventional WAAM is complex because the deposition is limited to flat surfaces. Therefore, a novel technique was used to deposit the NiTi track with WAAM on the rotatable cylindrical shaft to fabricate the prototype NiTi Belleville spring (Video F4). A stepper motor consisting of a chuck was connected to an Arduino microcontroller to rotate the chuck. A tapered cylindrical shaft was also installed in the chuck, and the assembly was held above the WAAM bed. Finally, a prototype of Belleville spring made of NiTi SMAs was produced by continuous linear motion of the WAAM nozzle over the rotating tapered shaft.

3. Materials characterization

A cross-section of a three-layered NiTi-deposited track and the appearance of the top bead deposited by WAAM with wires exhibiting SE and SM effects are shown in Fig. 2a. For simplicity, the tracks were numbered from bottom to top, i.e., the 1st track (T1) was deposited on the mild steel substrate, and the 3rd track (T3) was the last deposited track. The informed deposition of the track without having any discontinuity can be observed in Fig. 2a.

In addition, the as-built structure showed no signs of surface oxidation, as confirmed by energy dispersive spectroscopy (EDS) analysis. It is imperative when it comes to NiTi, as it is highly susceptible to oxidation at high temperatures, which degrades its mechanical and functional properties [7]. Since WAAM samples usually exhibit columnar grains in

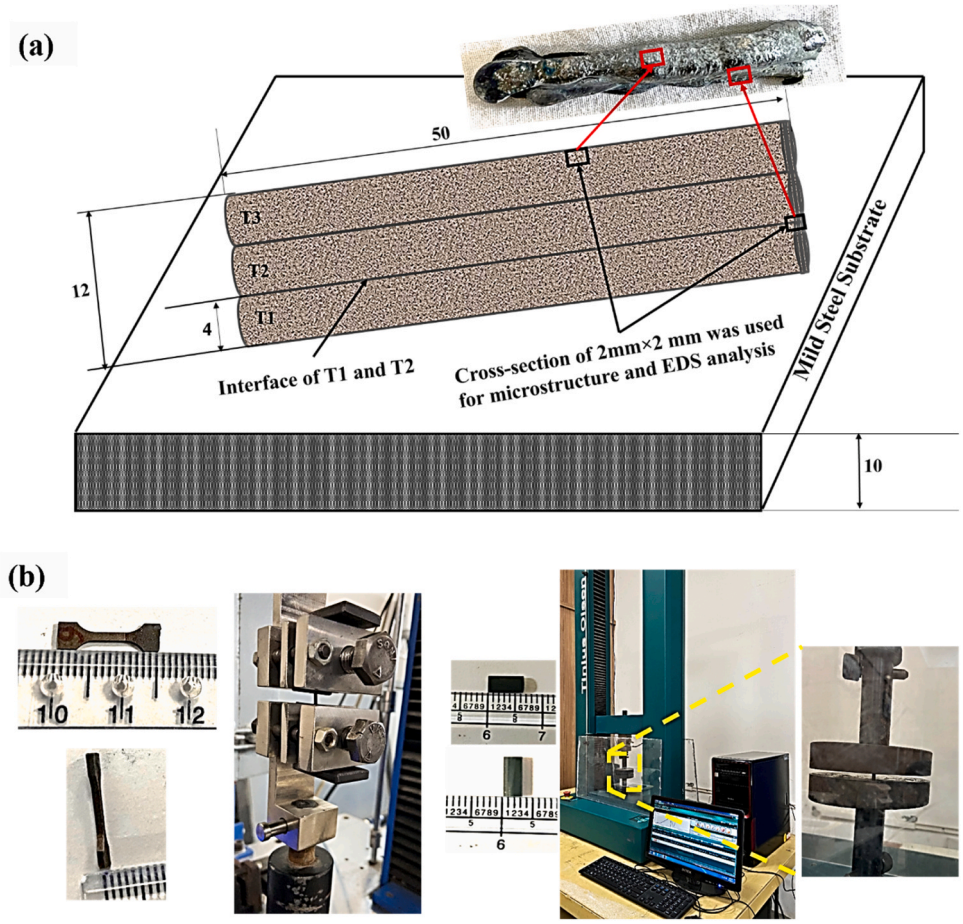

Fig. 2. (a) A schematic of the 3-layered NiTi part produced by WAAM and the location of the cross-sections cut for EDS and microstructure analysis; (b) Dog bone tensile specimens and compressive specimen along with the testing setup.

the intermediate region [33–35], the interface between the layers was investigated in this study. Additionally, previously reported literature showed the microstructural studies via interfaces and demonstrated the comparison between them. Therefore, the current analysis was performed at the interface between T1 and T2 and the top layer of T3. In addition, the prime objective of the present study is to make a Belleville spring. It was found further that the bottom layers were showing Fe pickups, which might contaminate the samples, so the top layer without any Fe content (depicted from the EDS study) was chosen for further studies. A cross-section of 2 mm × 2 mm cut from the interface of T1-T2 and T3 top layer for EDS and microstructure analysis. An optical microscope (Make and model: LOMO "Metam 31- LV") was used to obtain a panoramic macroscale view of the fabricated joint. The as-built samples were examined using SEM (Carl Zeiss-Merlin™) equipped with an EDS instrument (Oxfords Instruments INCAx-act). To perform microstructural analyses, the samples were ground till 3000 grit SiC abrasive paper, followed by colloidal silica polishing and etching using Kroll's reagent (H_2O, HNO_3, HF, 5:4:1) for 10–15 s. The elemental compositions were analyzed using EDS for both the NiTi wires and the WAAM deposited samples at the different interfaces of the tracks. The structure of the samples was also examined under ambient conditions using an X-ray diffraction apparatus (Bruker D8 DISCOVER diffractometer) at an interval of 2θ in the range of 30°– 80° with a CuKα radiation source (λ = 1.5406 Å). For performing the transmission electron microscopy (TEM), foil of 500-micron thickness was cut and subsequently reduced to 70-micron thickness via polishing. Discs of 3 mm diameter were punched out from this thin foil, followed by electropolishing using Kroll's reagent. These samples were further thinned using focused ion beam (FIB) milling. Identification of the precipitates was carried out using the selected area diffraction pattern (SAED) and high-resolution transmission electron microscope (HRTEM) (Tecnai G2). SAED patterns were analysed using the crystbox software (version 1.10).

The phase transformation characteristics of samples S1 and S2, deposited with SE and SM effect wires respectively, were determined with a differential scanning calorimeter (DSC). To investigate the martensitic transformations, a 2 mm × 2 mm miniature was cut from S1 and S2 using the wire electrical discharge machining (WEDM). The martensitic transformations were measured using a DSC (Mettler Toledo 822e) at a cooling and heating rate of 10 °C/min from − 100°C to 150°C.

The test specimens were prepared as per ISO 13314 [36] in a cylindrical shape of Ø 3 mm × 6 mm (see Fig. 2b) to determine the compressive strength of S1 and S2. Three sets of dog-bone shape (see Fig. 2b) specimens with dimensions of 5 mm (gauge length), 1 mm (thickness), and 3 mm (width) were drawn using WEDM to evaluate the tensile strength of the S1 and S2. A crosshead speed of 0.5 mm/min was used to perform compression and tension tests. A special inter-gripper was used for holding purpose of such a small specimen, which was attached to the standard grippers of the universal testing machine (Tinius Olsen-H50KL, 50 kN, USA) to test the sample until failure. A Vickers microhardness tester (Make and Model: WlterUhl-VMHT002) with a load of 1.96 N and a dwell time of 10 s was used to evaluate the microhardness.

The superelastic behavior of the deposited NiTi samples was analyzed using the cyclic loading test. Samples of cylindrical shapes with the size of Ø 3 mm × 4.5 mm were taken to perform the test. A strain rate of 1×10^{-3} s^{-1} was used to perform the tests. 10 kN of the load was applied to the sample, and then the sample was unloaded. In other words, 2%, 4%, 6%, and 8% pre-strain was applied to all the wire arc

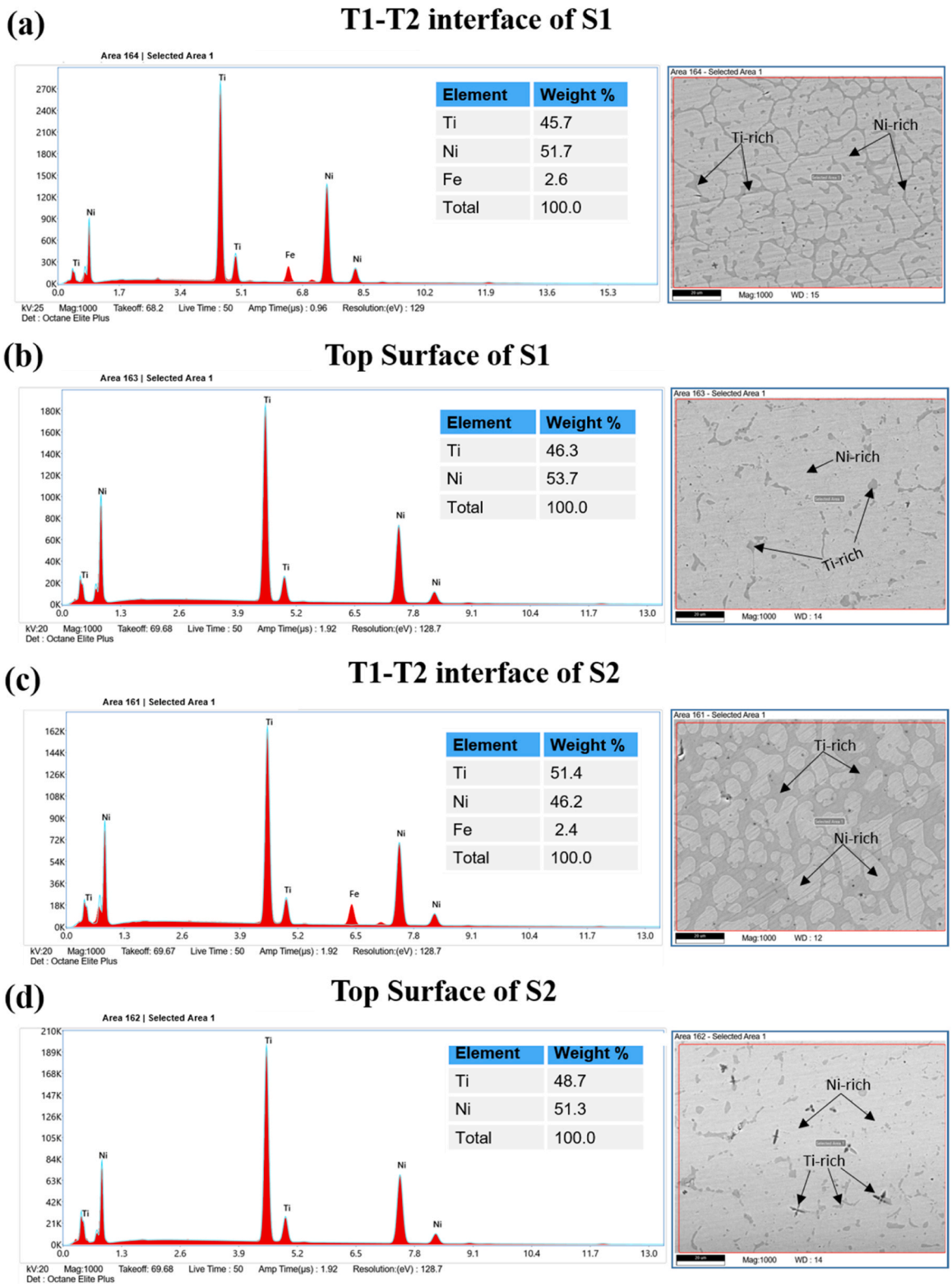

Fig. 3. Elemental analysis of S1 (a) at T1-T2 interface, (b); at top surface of T3; and S2 (c) at T1-T2 interface (d) at top surface of T3.

additively manufactured samples. The amount of recoverable and irrecoverable strains was recorded after the test to quantify the amount and percentage of the superelasticity.

4. Results and discussion

4.1. EDS analysis of deposited tracks

The elemental compositions of the NiTi wires and the WAAM deposited tracks were evaluated by EDS analysis. NiTi wires with an elemental composition of 53 wt% Ni and 47 wt% Ti, as the SE effect

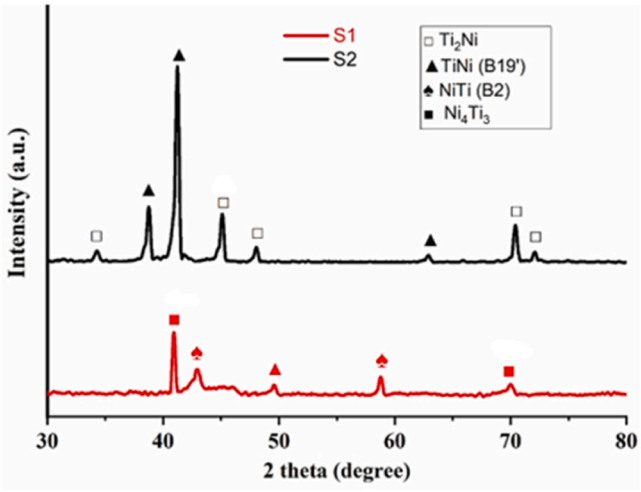

Fig. 4. XRD pattern of the T3 for both S1 and S2.

wire, whereas those with 51.2 wt% Ti and 48.8 wt% Ni, as SM effect wire, were taken in this study. Based on EDS results, as shown in Fig. 3, Ni content at the interface of T1-T2 For S1 was found to be 51.7 wt%, whereas for the top surface, it was 53.7 wt%. For S2, Ni composition was 46.2 wt% for the T1-T2 interface and 51.3 wt% at the top surface. In this context, it is essential to mention here that the matrix of sample S1 shows the presence of a higher amount of nickel, which can be evident from Fig. 3(a), which further increases with an increase in the further deposited layers. This variation in the nickel concentration inside the matrix of the deposited sample can be attributed to the lower melting point of the nickel that allows it to dissolve, and its concentration increases further while going up along the layers. In addition to that, it can be further noticed that the interface between the T1-T2 layer shows the peak of Fe in sample S1, which can be further correlated to the fact that the substrate used for the deposition of the nitinol was made of Fe and as a reason of which the first layer of nitinol deposited melts the substrate and picked up some amount of Fe from the substrate. However, the Fe vanishes while going up along the layers (top layer), which can be further attributed to the fact that the amount of Fe pickup reduces as a reason for deposition and remelting of the subsequent layers, and that inhibits the further transfer of the Fe from the bottom to the successive top layers. Due to the presence of this Fe in the T1 and T2 layers, the studies of the DSC and XRD are focused mainly on the T3 layer, as this layer showed the absence of any Fe and is suitable for the fabrication of the Belleville spring.

It can be further studied from the microstructure that the S1 shows the presence of coarse grain size microstructures with the presence of the larger size grains (25 μm) in the interface of T1 and T2 (Fig. 3a) while going up along the layers, this grain size reduces to 15 μm further and becomes finer which can be a result of dissolution of the nickel in the matrix, followed by dissolution of titanium from the grain boundaries and as a result of this competitive dissolution, a Ni-rich NiTi phase is observed with titanium present along the grain boundaries in the minor amounts. In this context, it is essential to mention that the current study correlates well with optical microstructural analysis. Furthermore, the amount of nickel at the T1-T2 interface and top interface for S1 was found to be 51.7% and 53.7%, respectively, while it was 46.2% and 51.3% for S2. The variations in Ni content may be due to local segregation next to the solidification, precipitation, or preferential evaporation [18].

The elemental composition of S1 and S2 at the T1-T2 interface is shown in Fig. 3a and c, which has a Ni content with some Fe. The presence of Fe in the NiTi track disappeared as the number of track deposits increased since no Fe content was found in the top layers S1 and S2. It is essential to mention here that for both S1 and S2, the content of nickel increases from the bottom to the top layers, and it can be attributed to the dissolution of nickel while going up along the layers. However, the addition in the Ni content from the bottom to the top layer was less for S2 than S1 since S2 was a shape memory alloy with lower amounts of nickel than the superelastic S1 system.

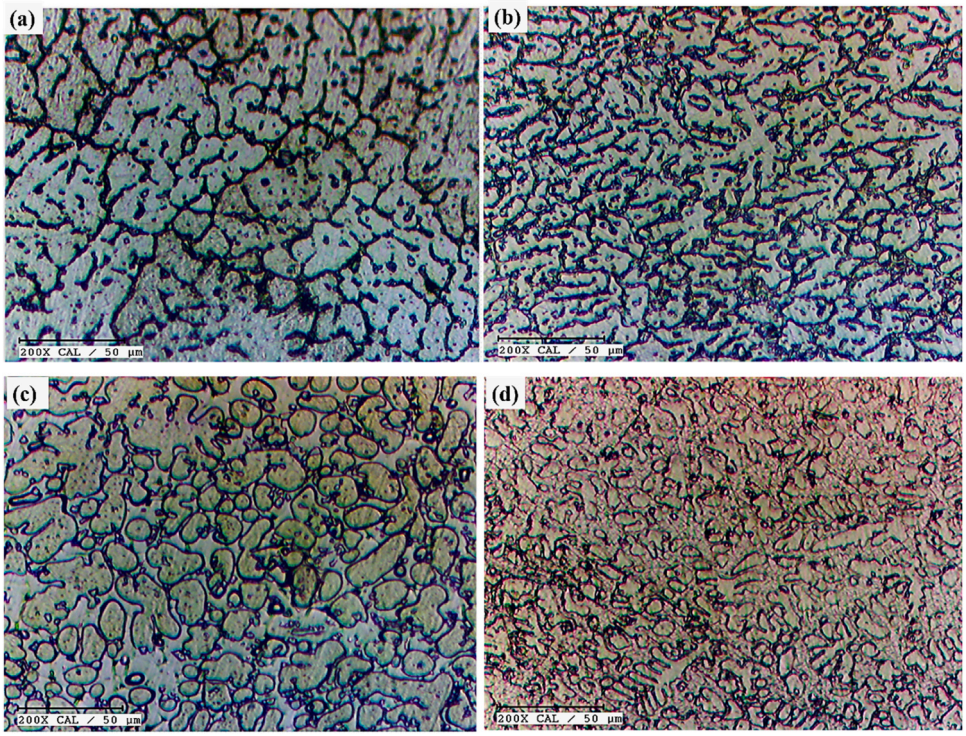

Fig. 5. Microstructure of S1 (a) at T1-T2 interface, (b) at the top surface T3, and S2 (c) at T1-T2 interface, (d) at the top surface T3.

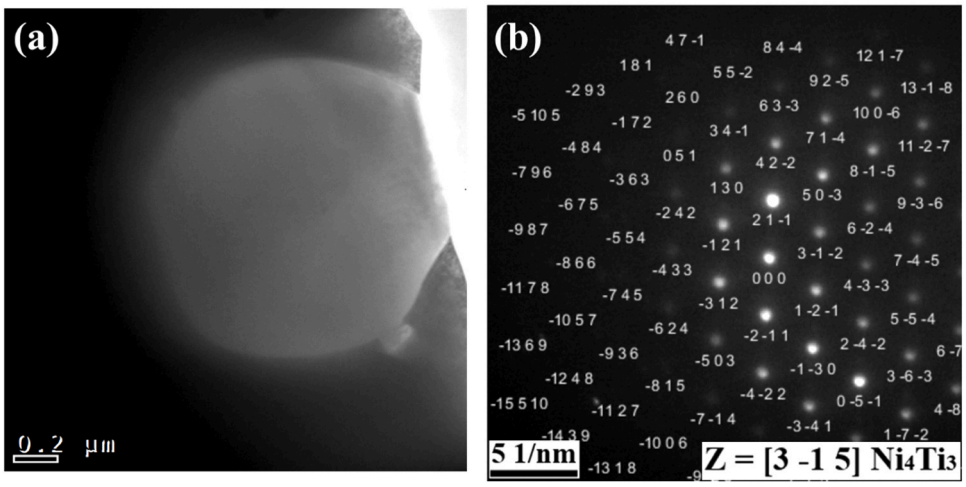

Fig. 6. (a) TEM bright field image of Ni_4Ti_3 (b) corresponding SAED pattern.

4.2. XRD analysis of deposited samples

It is well known that impurities like carbon, oxygen, ferrous, etc., affect the functional properties of SMA, so in the XRD study, only the top surfaces of S1 and S2 were taken for the phase analysis as no impurities were observed in these samples. At the same time, Fe was present for the T1 and T2 layers. The results of both S1 and S2 have been depicted in Fig. 4. It is evident from Fig. 4 that the sample produced using SE effect wire (S1) mainly consists of NiTi (B2 Austenitic) and a few NiTi (B19′ Martensitic) phase formations owing to complete inter-diffusion between elemental Ni and Ti.

For the sample S1 deposited using 53 wt% Ni composition, the formation of secondary phases of Ti_2Ni and Ni_4Ti_3 are shown, which may affect the mechanical properties due to the brittleness of the phases. It is well known that an increase in the Ni-content significantly increases the Ni_4Ti_3 phase in the matrix. Moreover, an increase in Ni-content also affects the features of the martensitic transformation of NiTi alloys [29]. As shown in Fig. 4, the increase in Ni content in the NiTi matrix, led to formation of the Ni-rich intermetallic compound Ni_4Ti_3 in the obtained NiTi sample.

Generally, the increase in Ni_4Ti_3 secondary phases in the NiTi matrix enhances the superelastic behavior of the material, which is mostly correlated with the critical stress required for the dislocation slip to occur. To add further, this precipitate enhances the hardening effect in the material by making it difficult for the dislocations to move freely. It raises the critical stress required for the plastic deformation to occur, thereby enhancing the superelasticity of the material. As a reason for the same, S1, with Ni_4Ti_3 in it, shows an enhanced superelastic recovery compared to S2. Furthermore, the sample S1 merely contains NiTi (B19′ Martensitic) phase, indicating the possibility of having more superelastic behavior in the sample compared to the sample with more martensitic phases in the matrix. However, sample S2 deposited with the composition of 48.8 wt% Ni wire, mostly forms secondary phases like Ti_2Ni and NiTi (B2) in the matrix. Since the sample deposited using SM effect wire (S2) possesses a greater number of Ti_2Ni phases in the matrix, which suppresses the superelastic characteristics of the sample as compared to the sample having a minimal number of the Ti_2Ni phases and a higher number of Ni_4Ti_3 phases in the matrix.

4.3. Microstructure characterization

Microstructural analysis has been performed on both shape memory and superelastic nitinol samples across different interfaces to study the evolution of the grain structures across the interface. Figs. 5a and 5b respectively depict the microstructural images of S1 obtained at the T1-T2 interface and the top surface of T3. It is known that the large surface area of the substrate enables rapid cooling due to better heat conduction of the first deposited layer, which results in a dendritic/tree-like microstructure for the samples deposited at the bottom layers, the morphology of these grains changes to become equiaxed in the 2nd deposited layer due to lower amount of the conduction area provided to the sample for cooling and it further decreases the thermal gradient due to lower cooling rates as a reason of the previously deposited layer that causes a partial remelting of the previously deposited dendritic grain layers and thereby forms equiaxed grains as the cooling rate slows down [22].

It is to be mentioned further that no inter-pass cooling is provided between two intermediate layer depositions as a reason why no cooling effect was provided to the sample, and thereby, this slow cooling rate leads to the evolution of such equiaxed grains from dendritic grains as evident from the microstructures. When the third layer is deposited over the 2nd layer, it can dissipate the stored heat via the layer below it. In addition to that, since no layer was deposited on top of this layer, this layer underwent air cooling that induces higher cooling rates within the sample and thereby produces a finer grain within the microstructures, as evident from Fig. 5b.

The corresponding microstructures of the sample S2 at the T1-T2 interface and the top surface of T3 have been shown in Figs. 5c and 5d. Similarly, due to the higher heat dissipation in T1, many dendritic grains were found at the T1-T2 interface. In the subsequent tracks, the dendritic tree-like microstructure became less and less. Due to a faster cooling rate than the previously deposited tracks, the top surface of T3 may have relatively fewer dendritic grains than T1-T2. Moreover, the grain size in T3 decreases significantly from T1 since no further depositions were made, and the time and temperature necessary for grain growth cannot be achieved in the final layer. Thus, it is feasible to state that the grain morphology differs in successive layers of NiTi due to different thermal cycle conditions, namely the decrease in cooling rate with consecutive layers, except that the deposited track was the last NiTi track. Furthermore, a secondary phase like $NiTi_2$ is vital in refining the microstructure during alloy processing. According to the XRD results, S2 has more $NiTi_2$ phases than S1, which could explain why it has a finer microstructure than S1.

TEM studies revealed the presence of second-phase precipitates in the sample and their corresponding SAD patterns shown in Fig. 6(a-b). Precipitates of lenticular disc shaped Ni_4Ti_3 precipitates were observed and confirmed further via the SAD pattern obtained from the precipitate. Submicron precipitation of Ni_4Ti_3 was evident from the micrographs with an average width of 800 nm, growing parallelly in specific angular relation with the grain boundary. The enhanced superelasticity for S1 is

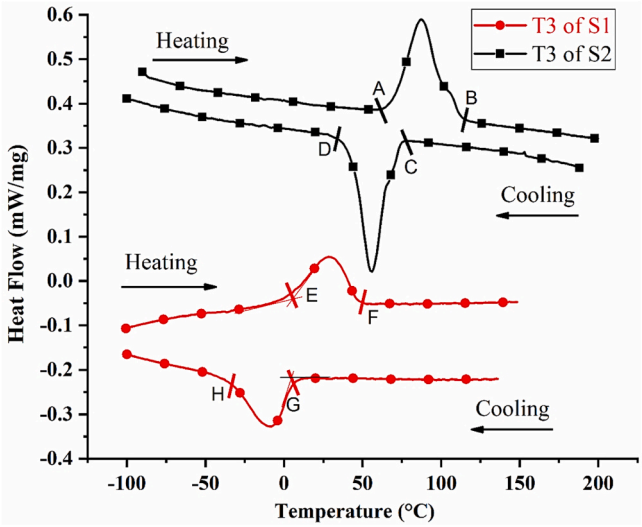

Fig. 7. Calorimetric curves of T3 for both S1 and S2 on heating and cooling.

attributed to the presence of the Ni_4Ti_3 as a reason for the same, and this phase is characterized and reported via TEM, while others are not.

4.4. Phase transformation characterization

NiTi has a high susceptibility to oxidation and impurities at high temperatures. Only the last track (T3) of S1 and S2 were taken to analyze their phase transformation properties since these samples contain only base elements, i.e., Ti and Ni, in their matrix. The results are depicted in Fig. 7. The details of the transformation temperatures are given in Table 2. Austenite and martensite are denoted by A and M, respectively, whereas the start and finish of transformation are denoted by the subscripts s and f, respectively.

Fig. 7 shows the calorimetric heating and cooling curve for both S1 and S2. It is evident from the figure that two peaks were observed in the heating and cooling cycles for both S1 and S2. The onset temperatures of 4.6 °C and 50.2 °C were reached in S1 for both M_s and A_f, respectively, indicating a wider transformation range and hysteresis compared to S2, which had onset temperatures of 73.1 °C and 114.8 °C, respectively. The differences in transformation temperatures depend on chemical compositions and precipitation like Ni_4Ti_3 [37].

The phase transformation results for the T1-T2 interface for both S1 and S2 were obtained (Supplementary Figure P1 and Table G1) fraction calculations were performed using the analysis for the T1-T2 interface and Top surface for both S1 and S2 (Supplementary figure P2).

It can be observed from the Fig. 3 study that Ni-rich regions are found in the grain interiors and grain boundaries showing the segregation of the Ti-rich regions as confirmed via EDS studies. Following this study, the phase fractions were calculated to check the amount of these regions (Figure P2). It has been obtained from Table G2 that a higher amount of Ni-rich matrix region was obtained for S1 in both T1-T2 interface (T1-T2-S1) and at the top surface (Top-S1) with 78.21% and 91.95% respectively compared to S2 where only 51.72% and 80.21% respectively values were reported. Conversely, a lower amount of Ti-rich regions were obtained for the sample S1 in both T1-T2 interface and the top surface with 21.79% and 8.05% compared to S2 with 48.28% and 19.79% respectively. It is important to mention that, a higher amount of Ni-rich regions in the matrix and lower Ti-rich grain boundary regions in the case of S1 at the top interface compared to S2 related to the segregation of Ti along the grain boundaries which enhances the chances of forming $NiTi_2$ phases for S2 and as a reason for the same a higher $NiTi_2$ phases were observed in case of S2 from XRD results (Fig. 4) [38,39]. It has been reported previously that the presence of this excessive Ni % promotes the formation of Ni-rich precipitates in the matrix and as a reason for the same the top surface and T1-T2 interface of S1 shows the presence of Ni-rich Ni_4Ti_3 precipitates from XRD (Fig. 4) and reduces the transformation temperatures to lower values and enhances the superelasticity [40]. Furthermore, for S1, at the top surface, transformation temperatures were lower than the room temperatures and B2 austenitic phase was expected and the same was obtained from the XRD results (Fig. 4 vis a vis Table 2). Furthermore, for both S1 and S2, transformation temperatures decreased with an increase in the deposition height from T1-T2 to top surface due to an increase in the Ni content within the matrix (Figure P1, P2 vis-à-vis Table G1, G2 vis-à-vis Table 2) as it is well known that 1 at% decrease in Ms temperature increases the transformation temperature by 100 °C and similar results were reported for nitinol previously [28,29]. However, the higher transformation temperatures were obtained for the top surface of S2 which can be attributed to the presence of $NiTi_2$ (Fig. 4) which gives rise to Marangoni convections to reduce the Ni content from the matrix [8]. In the current study, it can be observed that the presence of Ni_4Ti_3 in sample S1 shows a superelastic effect; it is also well-known that this Ni_4Ti_3 phase increases the superelastic behavior by altering the transformation temperature. This is why S1 in the DSC analysis shows higher superelastic behavior than S2.

Table 2
Transformation temperatures (°C) of the samples fabricated using WAAM with SE and SM effect NiTi wires.

Samples	A_s	A_f	M_s	M_f
S1	E = 5.8	F= 50.2	G= 4.6	H= −33.8
S2	A= 59.8	B= 114.8	C= 73.1	D= 33.9

Several factors may explain the variations in transformation behavior between NiTi alloys produced using WAAM with different Ni contents in the matrix. First, from the microstructural perspective, grain sizes, compositions, and residual stresses are expected to differ for both Ti-rich and Ni-rich nitinol alloys. The high Ni content in the matrix plays a significant role in the grain refinement of the matrix of NiTi alloys. It has been observed that NiTi alloys undergo martensitic transformation depending on their grain size variations [37,41]. Moreover, the residual stresses for the WAAM part are not uniform because the thermal cycling conditions vary from part to part. Oliveira et al. [42] have shown that the transformation behavior can vary significantly due to the generation of thermally induced residual stresses in NiTi under localized heat sources by processing through SLM or WAAM. In addition, the presence of Ni_4Ti_3 in this study may also affect the matrix's chemical composition due to nanoscale precipitation, which led to changes in transformation temperatures [43]. Previously, it was found that the SLM of NiTi formed nanoscale Ni_4Ti_3 [44]. As for the precipitation of Ni_4Ti_3, the SLM usually has a low thermal cycle compared to WAAM. Moreover, it can be assumed that the conditions favour the formation of Ni_4Ti_3 precipitates during the fabrication of the part due to the increasing heat accumulation. However, with WAAM, it takes only a few seconds for precipitation to start; however, the volume fraction is likely to be small [45].

From the above description, it can be inferred that there could be a variety of possible explanations for the different transformation characteristics of the NiTi part fabricated with WAAM. In the present study, the XRD results of the as-built parts showed a good correlation with the DSC analysis, indicating that the NiTi samples deposited with WAAM contain all types of austenite and martensite phases. One possible reason for the presence of Ni_4Ti_3 precipitates is the continuous reheating and cooling of the existing layers. It is known that the temperature ranges from 500 °C to 300 °C is optimal for the precipitation of Ni_4Ti_3 in only a few seconds [46]. Ultimately, the presence of Ni_4Ti_3 in the deposited NiTi components increases the depletion of Ni and thus justifies the increased transformation temperatures of the components produced with WAAM. Thereby, in the current study, variation of transformation temperature due to compositional variations of Ni and Ti distribution along the build height leads to formation of Ni and Ti rich regions within

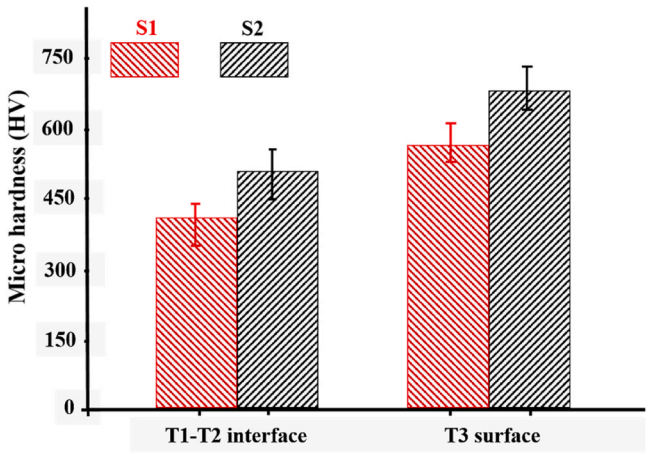

Fig. 8. Hardness of S1 and S2 at T1-T2 interface and at T3.

the system which furthermore leads to the formation of various secondary phases like $NiTi_2$ and Ni_4Ti_3 that further controls the superelasticity and other mechanical properties within the system.

4.5. Mechanical characterization

4.5.1. Comparison of a micro-hardness

The micro-hardness of the S1 and S2 were investigated, and their results have been depicted in Fig. 8. The T1-T2 interface of S1 and S2 shows a respective hardness of 430 HV 525 HV, while it was found to be 590 HV for S1 and 660 HV for S2 in the T3. The lower hardness at the T1-T2 interface can be attributed to dendritic grains and the distinct grain morphologies (Ref. Fig. 5). In contrast, the combination of fewer dendritic with primary equiaxed morphology in the last deposited track is accountable for the increased hardness [47,48]. Since the topmost layer was the last to be deposited and was cooled by the surroundings, it was subjected to a relatively higher cooling rate than the preceding deposited track, thus resulting in fewer columnar microstructures with finer grains. Furthermore, it is expected that the middle track should have fairly equiaxed grains, as the partially remelted grain occurs on the following deposit and does not allow the track to cool down immediately. Unlike other materials, such as steel, that undergo a martensitic transformation, the cooling rate does not significantly influence the resulting hardness. Moreover, it was also observed that every track of S2 contained higher hardness than the tracks of S1.

The main reason for the improvement in the hardness of every track of S2 than S1 is owing to an increase in the Ni depletion from the matrix, which resulted in the formation of many intermetallic compounds such as $NiTi_2$ precipitates in the NiTi phase, leading to a second phase

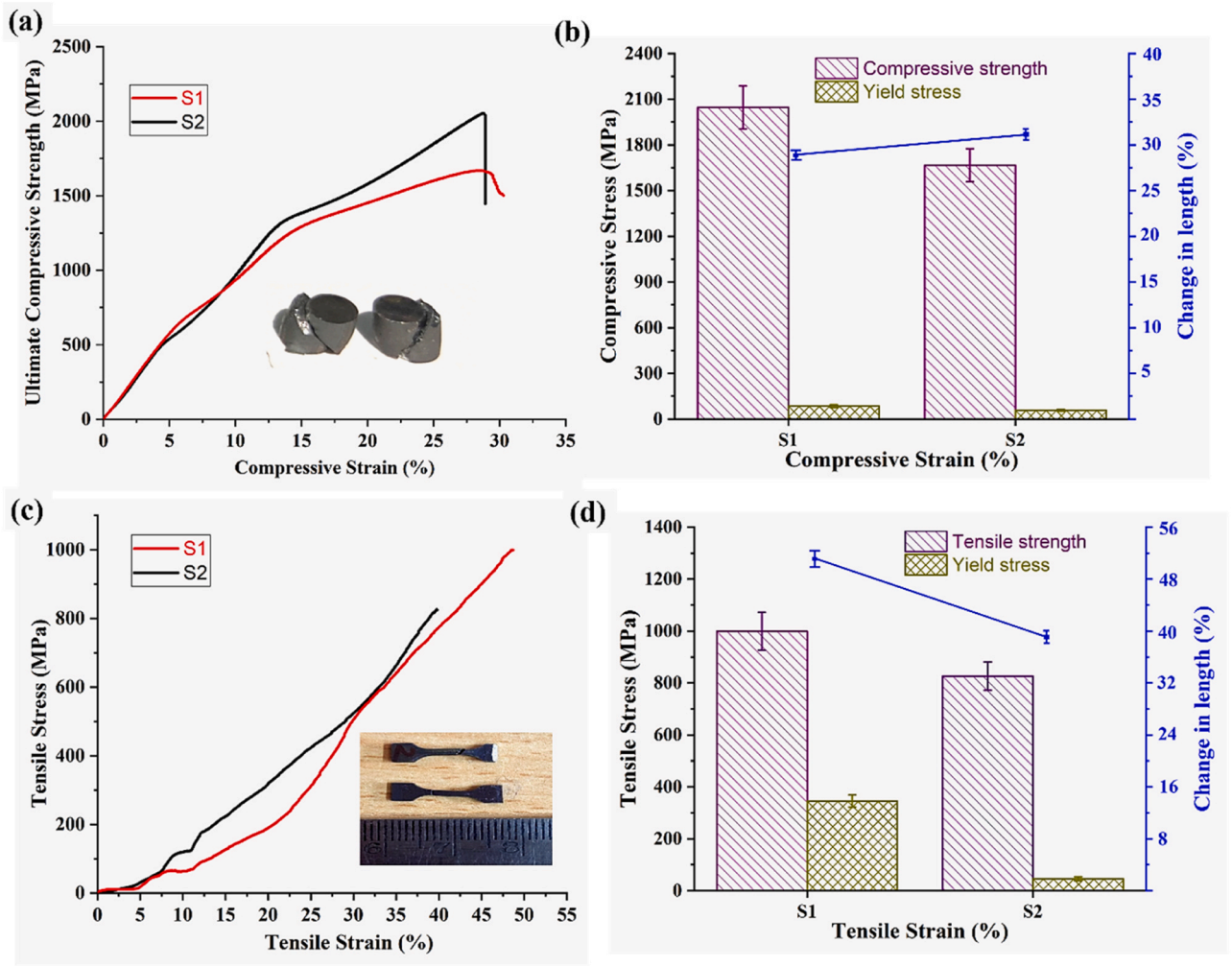

Fig. 9. (a) Compressive stress vs. strain, (b) compressive strength, yield stress, and % change in length, (c) tensile stress vs tensile strain, and (d) tensile strength, yield stress, and % change in length of samples obtained from T3 for both S1 and S2.

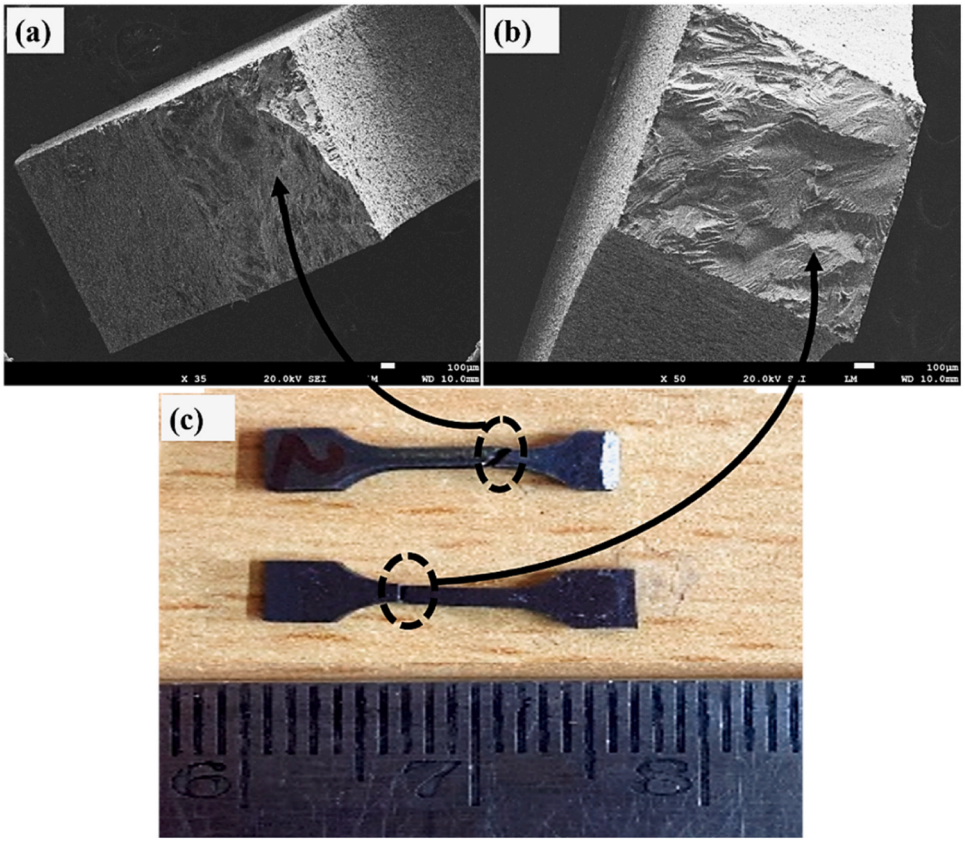

Fig. 10. SEM images of fractured samples (a) S1 and (b) S2.

strengthening effect. In addition to that, the Ti enrichment in the matrix leads to a further increase in the hardness effects for S2. According to XRD analysis, the production of the martensite phase is higher in the Ti-rich composition (S2) than in the Ni-rich composition (S1). This can be attributed to the fact that the S2 at room temperature consists mainly of a higher martensitic phase (B19′) with a mere amount of austenite (B2) for this system room temperature lies between its M_s and M_f temperatures as studied from the DSC and XRD studies (Fig. 4 vis-à-vis Fig. 7 vis-à-vis Table 2) and as a reason for the same shows a higher hardness compared to S1 for which room temperatures lies between A_s and A_f and thereby having majority of austenitic grains (B2) and mere amount of martensitic phases and thereby having a lower hardness compared to S2. These Ni-rich alloys are harder than Ti-rich alloys because more martensitic phase formation occurs in Ni-rich compositions.

4.5.2. *Comparison of compressive and tensile stress-strain*

Fig. 9a shows the compressive stress vs. strain of both S1 and S2. It was found that the S2 has higher compressive strength and lower elongation ability as compared to the S1 (Ref. Fig. 9b), which can be attributed to the presence of a higher amount of martensitic phases compared to S1, which shows the presence of a more elevated amount of austenite peaks as depicted from the XRD results as well (Fig. 4). It is well known that martensite has a higher compressive strength than austenite. To add further, austenite with an FCC structure shows a ductile nature with low compressive strength compared to martensite, where austenitic to martensitic transformation induces higher dislocation density and more significant lattice distortion, which increases the compressive strength of the system. In addition, the presence of Ti_2Ni phases and martensitic phases (B19′) in the NiTi matrix for S2 restricts the dislocation motions in the sample, and less deformation was obtained in the S2 compared to the S1.

Similarly, the tensile stress vs. strain of both S1 and S2 have been shown in Fig. 9c. In this case, it was found that the S1 has higher strength (yield and tensile) and elongation ability than the S2 (Ref. Fig. 9d). It is well known that the sample having higher brittle phases exhibits higher strength in compression and weaker in tension. So, this higher tensile strength in the S1 is due to forming a less brittle phase in the sample. Also, the relatively small amount of brittle phases in the S1 sample allowed the sample to elongate more in tensile loading than the S2 sample, which consisted of significant brittle phases.

4.5.3. *Fractography analysis*

After mechanical testing, the fractured sample was taken for the fractography study. Fig. 10 shows the SEM images of the fractured samples obtained after the tensile testing. A combination of ductile and brittle fracture was found in the S1 (Ref. Fig. 10a) as the fracture inclination was about 45°, indicating the presence of both ductility and brittleness in the sample [49-51]. In addition to that, the presence of shallow dimples with lower fineness and microvoids confirms the lower ductility for the S1 sample [52]. Further, the presence of austenite-rich phases with a mere amount of martensite in the microstructure, as evident from XRD (Fig. 4), depicts a mixed mode of fracture for S1. Fig. 10b represents a pure brittle fracture for the S2 as the inclination of the fracture was at the angle of 0°, which indicates the presence of mere brittleness in the sample. Moreover, S2 contained a significant amount of brittle phases like martensite, which was already confirmed by XRD analysis, and the same shows a brittle fracture compared to S1 with a higher amount of martensitic phases.

4.5.4. *Superelasticity test*

Fig. 11a-d shows the superelasticity effect of nitinol with a variation of pre-strain rate from (2−8) %. It can be observed from Fig. 11a-b that both the wires show almost equal amounts of strain recovery till the application of 4% of pre-strain. This elastic recovery starts to vary from Fig. 11c-d, where the S1 with a higher elastic recovery depicts a complete reversal to its initial loaded condition (98%) compared to the S2

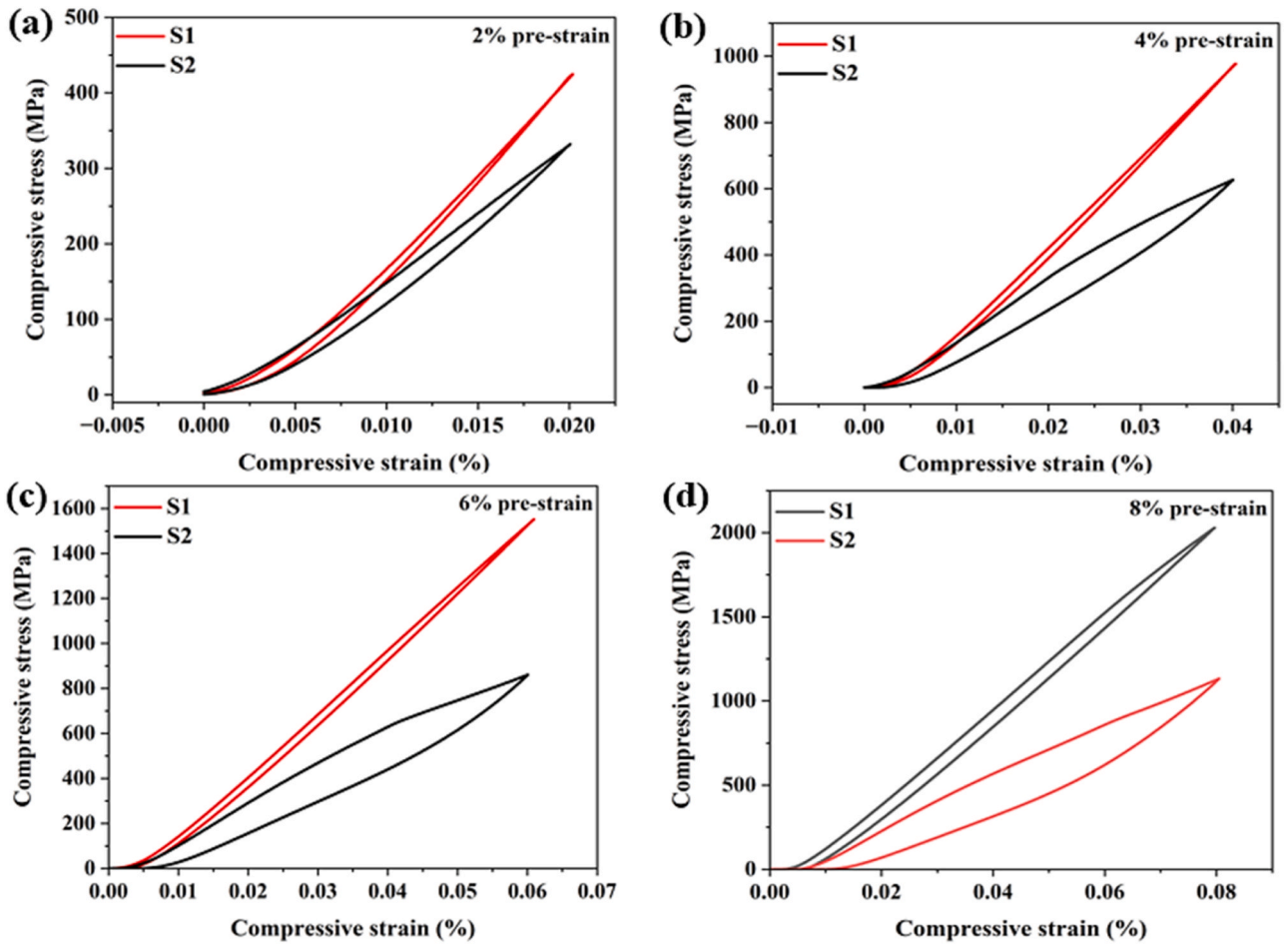

Fig. 11. Stress-strain curve obtained experimentally from printed WAAM nitinol samples with varying pre-strains of (a) 2% (b) 4% (c) 6% and (d) 8% for samples S1 and S2.

with a lower elastic recovery (66%) showing lesser superelasticity and thereby fails to revert to its initial shape and some irrecoverable plastic deformation stays within the material. This behavior can be correlated to the presence of Ni-rich phases like Ni_4Ti_3 within the microstructure as depicted from XRD results (Fig. 4) of superelastic nitinol, which results in a complete recovery of the applied deformation to the material when unloaded [34].

In addition to that, the inability of the S2 to achieve full elastic recovery after unloading can be attributed to the absence of phases like Ni_4Ti_3, which usually helps to achieve higher superelastic recoveries in the materials. So, microstructural variations along the build direction can explain the irrecoverable strain, and the sample, when tested at room temperature, also had some martensite a priory in the microstructure that can further lead to a decrease in the recovery of the strain as seen earlier [22]. It was reported earlier that the incoherent $NiTi_2$ phases fail to improve the superelasticity of the NiTi alloy, and the presence of this phase, in addition to the higher amount of martensitic phases in the case of S2, shows a lower amount of elastic recovery during unloading, of the sample. This $NiTi_2$ phase leads to the generation of a higher amount of inhomogeneous stress fields at the grain boundaries, which leads to the promotion of dislocation slip and thereby promotes further plastic deformation within the material and reduces the elastic recovery.

5. Conclusions

Wire and Arc Additive Manufacturing was used to fabricate NiTi shape memory alloy Belleville spring. Two types of commercially available NiTi wires, namely superelastic effect (SE) wire and shape memory (SM) effect wire, were taken as the feedstock material. To get the Belleville spring with its desired mechanical and functional properties, a comparative study of microstructure, phase transformations, and mechanical properties was performed between the WAAM samples deposited with SE effect and SM effect wires. The following main conclusions can be drawn:

i. SEM-EDS studies revealed increased Ni content towards T3 from the T1-T2 interface for S1 and S2. This increase in the Ni content from the bottom to the top layer was less for S2 than S1 since S2 was a shape memory alloy with lower amounts of nickel than the superelastic S1 system. XRD studies revealed the presence of different types of phases B2 austenite, B19′ martensite, and precipitates of $NiTi_2$, Ni_3Ti, and Ni_4Ti_3 for S1 and S2.
ii. Microstructural studies show dendritic microstructure at T1-T2 interface and equiaxed microstructure at T3 for both S1 and S2 with finer grains for S2 compared to S1 due to presence of $NiTi_2$ whereas S2 shows an increase in the Ni depletion from the matrix resulted in the formation of many intermetallic compounds, such as Ni_3Ti and $NiTi_2$ precipitates confirmed by XRD in the NiTi matrix, leading to a second phase strengthening effect in S1. The TEM studies confirm the presence of Ni_4Ti_3 for S1, which plays a critical role in improving superelasticity.
iii. Transformation temperatures from the DSC study show that onset temperatures of 4.6 °C and 50.2 °C were reached in S1 for both M_s and A_f, respectively, indicating a more comprehensive transformation range and hysteresis compared to S2, which had onset

temperatures of 73.1 °C and 114.8 °C. The increase in Ni content and the presence of Ni_4Ti_3 in the S1 drastically reduced the M_s and A_f temperatures, enhancing its superelasticity.

iv. Mechanical studies revealed a higher hardness (525 HV for T1-T2 interface and 660 HV for T3) and compressive strength for S2 as compared to S1, owing to the formation of more brittle precipitates and martensitic phases in the S1. The tensile strength and elongation were lower in the S2 sample than in the S1 due to lesser brittle degrees in the sample.

v. Fractography studies revealed more brittle fracture behavior for the S2 due to brittle phases and a mixed ductile-brittle fracture for the S1 with evidence of dimples and microvoids.

vi. S1 showed a significantly higher recoverable strain (98%) than S2 (66%) and demonstrated excellent superelastic properties at varying restrain from (2-8) % required for Belleville spring. By performing the comparative study between microstructure, mechanical, and phase transformation characteristics of samples manufactured using WAAM with superelastic effect NiTi wire (S1) and shape memory effect NiTi wire (S2), it was found that sample S1 has more suitable properties than S2 to manufacture the Belleville spring using WAAM due to its enhanced superelasticity due to presence of Ni_4Ti_3 obtained from the study compared to S1.

CRediT authorship contribution statement

Ajit Kumar: Conceptualization, Methodology, Investigation, Formal analysis, Writing – original draft. **Iyamperumal Anand Palani:** Supervision, Formal analysis, Writing – review & editing. **Muralidhar Yadav:** Formal analysis, Writing – review & editing.

Declaration of Competing Interest

The authors declare that they have no known competing financial interests or personal relationships that could have appeared to influence the work reported in this paper.

Data Availability

Data will be made available on request. All data that support the findings of this study are included within the article (and in supplementary files).

Acknowledgements

The authors are grateful to the research scholars of the Mechanical Engineering Department, IIT Indore, for their support. The research was financially supported by a joint DST-RSF project (RSF # 19-49-02014, DST #DST/INT/RUS/RSF/P-36).

Appendix A. Supporting information

Supplementary data associated with this article can be found in the online version at doi:10.1016/j.mtcomm.2023.107881.

References

[1] K. Otsuka, X. Ren, Physical metallurgy of Ti-Ni-based shape memory alloys, Prog. Mater. Sci. 50 (2005) 511–678, https://doi.org/10.1016/j.pmatsci.2004.10.001.
[2] J. Mohd Jani, M. Leary, A. Subic, M.A. Gibson, A review of shape memory alloy research, applications and opportunities, Mater. Des. 56 (2014) 1078–1113, https://doi.org/10.1016/j.matdes.2013.11.084.
[3] L. Petrini, F. Migliavacca, Biomedical Applications of Shape Memory Alloys, J. Metall. 2011 (2011) 1–15, https://doi.org/10.1155/2011/501483.
[4] N. Resnina, I.A. Palani, S. Belyaev, S. Singh, A. Kumar, R. Bikbaev, A. Sahu, Functional Properties of the Multilayer NiTi Alloy Produced by Wire Arc Additive Manufacturing, Shape Mem. Superelasticity. 8 (2022) 5–15, https://doi.org/10.1007/s40830-022-00359-0.
[5] M. Dolce, D. Cardone, Mechanical behaviour of shape memory alloys for seismic applications 2. Austenite NiTi wires subjected to tension, Int. J. Mech. Sci. 43 (2001) 2657–2677, https://doi.org/10.1016/S0020-7403(01)00050-9.
[6] V. Torra, A. Isalgue, G. Carreras, F.C. Lovey, H. Soul, P. Terriault, L. Dieng, Experimental study of damping in civil engineering structures using smart materials (NiTi - SMA). Application to stayed cables for bridges, Int. Rev, Mech. Eng. 4 (2010) 601–611.
[7] M. Elahinia, N. Shayesteh Moghaddam, M. Taheri Andani, A. Amerinatanzi, B. A. Bimber, R.F. Hamilton, Fabrication of NiTi through additive manufacturing: A review, Prog. Mater. Sci. 83 (2016) 630–663, https://doi.org/10.1016/j.pmatsci.2016.08.001.
[8] L. Yu, K. Chen, Y. Zhang, J. Liu, L. Yang, Y. Shi, Microstructures and mechanical properties of NiTi shape memory alloys fabricated by wire arc additive manufacturing, J. Alloy. Compd. 892 (2022), 162193, https://doi.org/10.1016/j.jallcom.2021.162193.
[9] H. Gugel, A. Schuermann, W. Theisen, Laser welding of NiTi wires, 668–671, Mater. Sci. Eng. A. (2008) 481–482, https://doi.org/10.1016/j.msea.2006.11.179.
[10] Z. Zeng, B. Panton, J.P. Oliveira, A. Han, Y.N. Zhou, Dissimilar laser welding of NiTi shape memory alloy and copper, (2015).
[11] H. Sahasrabudhe, R. Harrison, C. Carpenter, A. Bandyopadhyay, Stainless steel to titanium bimetallic structure using LENS^{T}M, Addit. Manuf. 5 (2015) 1–8, https://doi.org/10.1016/j.addma.2014.10.002.
[12] B. Tam, A. Pequegnat, M.I. Khan, Y. Zhou, Resistance microwelding of Ti-55.8 wt pct ni nitinol wires and the effects of pseudoelasticity, Metall. Mater. Trans. A Phys. Metall. Mater. Sci. 43 (2012) 2969–2978, https://doi.org/10.1007/s11661-012-1115-7.
[13] D.T. Waghmare, C. Kumar Padhee, R. Prasad, M. Masanta, NiTi coating on Ti-6Al-4V alloy by TIG cladding process for improvement of wear resistance: Microstructure evolution and mechanical performances, J. Mater. Process. Technol. 262 (2018) 551–561, https://doi.org/10.1016/j.jmatprotec.2018.07.033.
[14] W. Zhang, S.S. Ao, J.P. Oliveira, Z. Zeng, Z. Luo, Z.Z. Hao, Effect of ultrasonic spot welding on the mechanical behaviour of NiTi shape memory alloys, Smart Mater. Struct. 27 (2018), https://doi.org/10.1088/1361-665X/aacfeb.
[15] W. Zhang, S. Ao, J.P. Oliveira, C. Li, Z. Zeng, A. Wang, Z. Luo, On the metallurgical joining mechanism during ultrasonic spot welding of NiTi using a Cu interlayer, Scr. Mater. 178 (2020) 414–417, https://doi.org/10.1016/j.scriptamat.2019.12.012.
[16] M. Taheri Andani, S. Saedi, A.S. Turabi, M.R. Karamooz, C. Haberland, H. E. Karaca, M. Elahinia, Mechanical and shape memory properties of porous Ni50.1Ti49.9 alloys manufactured by selective laser melting, J. Mech. Behav. Biomed. Mater. 68 (2017) 224–231, https://doi.org/10.1016/j.jmbbm.2017.01.047.
[17] B. Zhang, W.J. Meng, S. Shao, N. Phan, N. Shamsaei, Effect of heat treatments on pore morphology and microstructure of laser additive manufactured parts, Mater. Des. Process. Commun. 1 (1) (2019) 8, https://doi.org/10.1002/mdp2.29.
[18] K.F. Ayarkwa, S.W. Williams, J. Ding, Assessing the effect of TIG alternating current time cycle on aluminium wire + arc additive manufacture, Addit. Manuf. 18 (2017) 186–193, https://doi.org/10.1016/j.addma.2017.10.005.
[19] M. Dinovitzer, X. Chen, J. Laliberte, X. Huang, H. Frei, Effect of wire and arc additive manufacturing (WAAM) process parameters on bead geometry and microstructure, Addit. Manuf. 26 (2019) 138–146, https://doi.org/10.1016/j.addma.2018.12.013.
[20] X. Xu, J. Ding, S. Ganguly, S. Williams, Investigation of process factors affecting mechanical properties of INCONEL 718 superalloy in wire + arc additive manufacture process, J. Mater. Process. Technol. 265 (2019) 201–209, https://doi.org/10.1016/j.jmatprotec.2018.10.023.
[21] M.H. Elahinia, M. Hashemi, M. Tabesh, S.B. Bhaduri, Manufacturing and processing of NiTi implants: A review, Prog. Mater. Sci. 57 (2012) 911–946, https://doi.org/10.1016/j.pmatsci.2011.11.001.
[22] Z. Zeng, B.Q. Cong, J.P. Oliveira, W.C. Ke, N. Schell, B. Peng, Z.W. Qi, F.G. Ge, W. Zhang, S.S. Ao, Wire and arc additive manufacturing of a Ni-rich NiTi shape memory alloy: Microstructure and mechanical properties, Addit. Manuf. 32 (2020), https://doi.org/10.1016/j.addma.2020.101051.
[23] T.A. Rodrigues, V. Duarte, J.A. Avila, T.G. Santos, R.M. Miranda, J.P. Oliveira, Wire and arc additive manufacturing of HSLA steel: Effect of thermal cycles on microstructure and mechanical properties, Addit. Manuf. 27 (2019) 440–450, https://doi.org/10.1016/j.addma.2019.03.029.
[24] Shalini Singh, Elena Demidova, Natalia Resnina, Sergey Belyaev, I.A. Palani, C.P. Paul, Ajit Kumar, and K.G. Prashanth.Mechanical Properties, Microstructure, and Actuation Behavior of Wire Arc Additive Manufactured Nitinol: Titanium Bimetallic Structures.3D Printing and Additive Manufacturing. ahead of print http://doi.org/10.1089/3dp.2021.0324.
[25] K.S. Derekar, A review of wire arc additive manufacturing and advances in wire arc additive manufacturing of aluminium, Mater. Sci. Technol. (U. Kingd.). 34 (2018) 895–916, https://doi.org/10.1080/02670836.2018.1455012.
[26] C.V. Haden, G. Zeng, F.M. Carter, C. Ruhl, B.A. Krick, D.G. Harlow, Wire and arc additive manufactured steel: Tensile and wear properties, Addit. Manuf. 16 (2017) 115–123, https://doi.org/10.1016/j.addma.2017.05.010.
[27] R. Sun, L. Li, Y. Zhu, W. Guo, P. Peng, B. Cong, J. Sun, Z. Che, B. Li, C. Guo, L. Liu, Microstructure, residual stress and tensile properties control of wire-arc additive manufactured 2319 aluminum alloy with laser shock peening, J. Alloy. Compd. 747 (2018) 255–265, https://doi.org/10.1016/j.jallcom.2018.02.353.
[28] J. Wang, Z. Pan, G. Yang, J. Han, X. Chen, H. Li, Location dependence of microstructure, phase transformation temperature and mechanical properties on Ni-rich NiTi alloy fabricated by wire arc additive manufacturing, Mater. Sci. Eng. A. 749 (2019) 218–222, https://doi.org/10.1016/j.msea.2019.02.029.

[29] M.I. Khan, A. Pequegnat, Y.N. Zhou, Multiple memory shape memory alloys, Adv. Eng. Mater. 15 (2013) 386–393, https://doi.org/10.1002/adem.201200246.
[30] N. Resnina, I.A. Palani, S. Belyaev, S.S.M. Prabu, P. Liulchak, U. Karaseva, M. Manikandan, S. Jayachandran, V. Bryukhanova, A. Sahu, R. Bikbaev, Structure, martensitic transformations and mechanical behaviour of NiTi shape memory alloy produced by wire arc additive manufacturing, J. Alloy. Compd. 851 (2021), 156851, https://doi.org/10.1016/j.jallcom.2020.156851.
[31] I. Ponikarova, I.A. Palani, P. Liulchak, N. Resnina, S. Singh, S. Belyaev, S.S. Mani Prabu, S. Jayachandran, V. Kalganov, A. Sahu, R. Bikbaev, U. Karaseva, The effect of substrate and arc voltage on the structure and functional behaviour of NiTi shape memory alloy produced by wire arc additive manufacturing, J. Manuf. Process. 70 (2021) 132–139, https://doi.org/10.1016/j.jmapro.2021.08.026.
[32] S. Singh, N. Resnina, S. Belyaev, A.N. Jinoop, A. Shukla, I.A. Palani, C.P. Paul, K. S. Bindra, Investigations on NiTi shape memory alloy thin wall structures through laser marking assisted wire arc based additive manufacturing, J. Manuf. Process. 66 (2021) 70–80, https://doi.org/10.1016/j.jmapro.2021.04.004.
[33] C.R. Cunningham, J.M. Flynn, A. Shokrani, V. Dhokia, S.T. Newman, Invited review article: Strategies and processes for high quality wire arc additive manufacturing, Addit. Manuf. 22 (2018) 672–686, https://doi.org/10.1016/j.addma.2018.06.020.
[34] B. Wu, Z. Pan, D. Ding, D. Cuiuri, H. Li, J. Xu, J. Norrish, A review of the wire arc additive manufacturing of metals: properties, defects and quality improvement, J. Manuf. Process. 35 (2018) 127–139, https://doi.org/10.1016/j.jmapro.2018.08.001.
[35] J. Wang, X. Lin, J. Wang, H. Yang, Y. Zhou, C. Wang, Q. Li, W. Huang, Grain morphology evolution and texture characterization of wire and arc additive manufactured Ti-6Al-4V, J. Alloy. Compd. 768 (2018) 97–113, https://doi.org/10.1016/j.jallcom.2018.07.235.
[36] 13314:2011(E) ISO, International standard mechanical testing of metals – ductility testing – compression test for porous and cellular metals. Geneva: ISO, 13314:2011 (E), 2011. ⟨https://www.iso.org/standard/53669.html⟩.
[37] J. Il'czuk, H. Morawiec, Effect of dislocation inhomogeneity on the martensitic transformation in NiTi alloys, Met. Sci. Heat. Treat. 40 (1998) 152–154, https://doi.org/10.1007/bf02471771.
[38] B. Li, L. Wang, B. Wang, D. Li, J.P. Oliveira, R. Cui, J. Yu, L. Luo, R. Chen, Y. Su, J. Guo, H. Fu, Tuning the microstructure, martensitic transformation and superelastic properties of EBF3-fabricated NiTi shape memory alloy using interlayer remelting, Mater. Des. 220 (2022), 110886, https://doi.org/10.1016/j.matdes.2022.110886.
[39] F. Mohammadi, M. Kharaziha, A. Ashrafi, Role of Heat Treatment on the Fabrication and Electrochemical Property of Ordered TiO2 Nanotubular Layer on the As-Cast NiTi, Met. Mater. Int. 25 (2019) 617–626, https://doi.org/10.1007/s12540-018-00228-5.
[40] S. Dadbakhsh, B. Vrancken, J.P. Kruth, J. Luyten, J. Van Humbeeck, Texture and anisotropy in selective laser melting of NiTi alloy, Mater. Sci. Eng. A. 650 (2016) 225–232, https://doi.org/10.1016/j.msea.2015.10.032.
[41] A. Ahadi, Q. Sun, Effects of grain size on the rate-dependent thermomechanical responses of nanostructured superelastic NiTi, Acta Mater. 76 (2014) 186–197, https://doi.org/10.1016/j.actamat.2014.05.007.
[42] J.P. Oliveira, F.M. Braz Fernandes, R.M. Miranda, N. Schell, J.L. Ocaña, Effect of laser welding parameters on the austenite and martensite phase fractions of NiTi, Mater. Charact. 119 (2016) 148–151, https://doi.org/10.1016/j.matchar.2016.08.001.
[43] G. Liu, S. Zhou, P. Lin, X. Zong, Z. Chen, Z. Zhang, L. Ren, Analysis of microstructure, mechanical properties, and wear performance of NiTi alloy fabricated by cold metal transfer based wire arc additive manufacturing, J. Mater. Res. Technol. 20 (2022) 246–259, https://doi.org/10.1016/j.jmrt.2022.07.068.
[44] J. Ma, B. Franco, G. Tapia, K. Karayagiz, L. Johnson, J. Liu, R. Arroyave, I. Karaman, A. Elwany, Spatial control of functional response in 4D-printed active metallic structures, Sci. Rep. 7 (2017) 1–8, https://doi.org/10.1038/srep46707.
[45] J.P. Oliveira, F.M. Braz Fernandes, R.M. Miranda, N. Schell, On the Mechanisms for Martensite Formation in YAG Laser Welded Austenitic NiTi, Shape Mem. Superelasticity. 2 (2016) 114–120, https://doi.org/10.1007/s40830-016-0058-z.
[46] A.R. Pelton, J. DiCello, S. Miyazaki, Optimisation of processing and properties of medical grade Nitinol wire, Minim. Invasive Ther. Allied Technol. 9 (2000) 107–118, https://doi.org/10.3109/13645700009063057.
[47] Z. Qi, B. Qi, B. Cong, H. Sun, G. Zhao, J. Ding, Microstructure and mechanical properties of wire + arc additively manufactured 2024 aluminum alloy components: As-deposited and post heat-treated, J. Manuf. Process. 40 (2019) 27–36, https://doi.org/10.1016/j.jmapro.2019.03.003.
[48] L. Wang, J. Xue, Q. Wang, Correlation between arc mode, microstructure, and mechanical properties during wire arc additive manufacturing of 316L stainless steel, Mater. Sci. Eng. A. 751 (2019) 183–190, https://doi.org/10.1016/j.msea.2019.02.078.
[49] A. Kumar, P. Pandey, Statistical modelling of mechanical properties and bio-corrosion behaviour of Mg3Zn1Ca15Nb fabricated using microwave sintering, J. Alloy. Compd. 854 (2020), 156211, https://doi.org/10.1016/j.jallcom.2020.156211.
[50] A. Kumar, P.M. Pandey, Study of the influence of microwave sintering parameters on the mechanical behaviour of magnesium-based metal matrix composite, Proc. Inst. Mech. Eng. Part C. J. Mech. Eng. Sci. 235 (2021) 2416–2425, https://doi.org/10.1177/0954406220951236.
[51] A. Kumar, P.M. Pandey, Effect of ultrasonic assisted sintering on mechanical properties and degradation behaviour of Mg15Nb3Zn1Ca biomaterial, J. Magnes. Alloy 9 (2021) 1989–2008, https://doi.org/10.1016/j.jma.2020.11.006.
[52] S.K. Ghosh, M. Yadav, Effect of thermal ageing on microstructure, mechanical properties, and fracture behaviour of 50% cold rolled duplex stainless steel (alloy 2507), Materwiss. Werksttech. 54 (2023) 676–692, https://doi.org/10.1002/mawe.202200231.